The International Journal of Advanced Manufacturing Technology (2019) 103:3479–3493
https://doi.org/10.1007/s00170-019-03707-0

ORIGINAL ARTICLE

Mechanical performance of carbon fiber/epoxy composites cured by self-resistance electric heating method

Shuting Liu[1] · Yingguang Li[1] · Yan Shen[1] · Yong Lu[2]

Received: 7 November 2018 / Accepted: 7 April 2019 / Published online: 6 May 2019

Abstract
Carbon fiber reinforced plastic self-resistance electric (SRE) heating has been conceived as an alternative to out-of-autoclave technology due to its characteristics of uniform heating, fast heating/cooling, low energy consumption, and low equipment investment. In this work, a series of SRE heating experiments were conducted, in which the temperature distribution field, energy consumption, and curing time of SRE curing process were characterized. Comprehensive mechanical tests and microscopic characterization were carried out. The experimental results exhibit that the rapid heating rate of SRE curing process resulted in a weaker matrix performance because of the insufficient time of void elimination, which finally leads to an inferior compression and flexural strength for the composite part, while the fiber preferential heating effect can significantly improve the fiber-resin interfacial strength, because the naturally formed temperature difference along the interfacial area enhanced the adhesive strength of the resin around the interface, which improved the macroscopic tension and interlaminar shear strength.

Keywords Polymer matrix composites (PMCs) · Self-resistance electric heating · Curing · Mechanical performance

1 Introduction

Carbon fiber reinforced plastic (CFRP) is one of the key engineering materials of the twenty-first century, which has been substantially used in various industrial applications due to the superior specific strength and stiffness. Especially in transportation industries, for pursuing the green, energy-saving, and efficient production mode, the imperative requirement of lightweight products has been promoting the continuous development of CFRP application [1, 2].

In the manufacturing processes of CFRP parts, the curing stage is the most crucial process to determine product qualities, which however needs the highest energy consumption, longest cycle, and most expensive operation cost [3, 4]. At present, the curing process of high-performance CFRP mainly relies on thermal curing, among which the autoclave curing has the highest curing quality because the curing condition of high temperature and pressure can ensure the excellent solidification and compactness of CFRP [5]. In the aerospace industry, over 98% of aerospace-grade CFRP parts are cured by autoclave curing process [6]. Nevertheless, a series of problems with thermal curing have forced technicians to reconsider the sustainability of this technology. Most importantly, the principle of thermal curing regarding the heat transferring from an external region to the inner material inevitably leads to a significant temperature gradient through the thickness of CFRP parts [7], which has been a key technical problem in this field. Besides, for ensuring temperature uniformity, thermal curing has to slow the heating rate and use plenty of dwellings, which require long curing cycle [8] and high energy consumption [9, 10].In addition, especially for autoclave curing technology, the initial equipment investment of large pressure vessels results in extreme high costs [3, 11, 12]. Hence, a large amount of effort has been put into developing alternative curing technologies, focusing on fabricating high-performance CFRP parts with short production cycle and low energy consumption.

In recent years, novel curing technologies such as microwave [13, 14] and induction heating [15, 16] have attracted wide attentions from scholars or enterprises in this field. To the different extent, above technologies can achieve the goal of low energy consumption, short curing period, and enhanced curing properties, but there are still certain problems

✉ Yingguang Li
liyingguang@nuaa.edu.cn

[1] College of Mechanical and Electrical Engineering, Nanjing University of Aeronautics and Astronautics, Nanjing 210016, China

[2] Department of Mechanical Engineering, Nanjing Institute of Technology, Nanjing, China

in these technologies. Generally, not all of the CFRP parts can be dealt with by these technologies. For example, microwave heating is unable to heat the multidirectional stacked CFRP laminates because of the electromagnetic shielding effect [6], and it also has limitations of penetration depth along thickness direction even for the unidirectional CFRP laminate [17]. Further, induction heating can only heat the CFRP parts that form closed vortex loops [18] in a particular area that depends on the coil size. In addition, high cost of equipment investment is required for some of above technologies due to the special heating cavities and the harmful radiation protection systems [3, 19]. In general, no matter what the pathway of energy access is, most of above curing methods actually are based on the final joule loss effect generated by electromagnetic induction inside the carbon fiber.

Directly conducting the electrical current to the carbon fiber by using electrodes, and heating the surrounding resin by the generated joule heat is supposed to be the simpler and more efficient way to achieve the electrical loss heating of CFRP itself. Up to the present, this heating technology has been reported occasionally in different expression forms, such as joule heating [21], resistance heating [22, 44], self-heating [32], and embedded heating [33]. In this article, in order to express this technology intuitively, the authors name it self-resistance electric (SRE) heating/curing. There are some advantages of the CFRP SRE heating/curing technology:

1. Absolute volumetric heating pattern results in a uniform temperature distribution as long as every single carbon fiber is conducted by electrical current [20].
2. The rapid heating and cooling rate are achieved due to the sensitive response of the temperature to the electrical current inside the carbon fiber [21].
3. High energy efficiency is reached because all the input electrical energy is used for heating CFRP itself, except for the controllable heat dissipation (if use the insulating layer) [22].
4. Only the power supply and mold are needed, so the curing equipment is considerably simplified compared to thermal curing or autoclaves processes [23].

However, despite the above advantages, there are still no mature applications of SRE heating/curing technology having been reported in literature or industries. The mechanical performance of final cured parts is supposed to be one of the basic evaluation criterion for a new curing process. Since 1990 to 2018, different types of mechanical properties for SRE cured samples have been investigated by 13 researches, as shown in Table 1. The mechanical property results of parts processed by SRE heating and traditional methods are listed in chronological order. In general, SRE heating studies for thermosetting or thermoplastic composite [27], continuous fiber or short fiber mat [36], and carbon fiber (CF) or glass fiber (GF) embedded carbon fiber layer [34] are all included in the table. Processes of laminates curing, joints adhesion [31, 35], and scarf repairing [33], etc. are reviewed, but the resistance welding processes are not within the scope. Specifically, tensile strength was the most widely investigated property, followed by flexural strength. Among 13 studies, 5 of them considered the strength of SRE process to be higher than that of traditional techniques, but 5 lower, and 3 did not carry out the comparative experiments. For comparison of modulus, only 3 of them thought the modulus were increased by the SRE heating, and 4 obtained the opposite results. Therefore, it can be concluded that, for some reasons, the existing research results on the mechanical properties of SRE curing process were inconsistent. In studies [25–28] from the 1990s to 2010, it was believed that the mechanical performance of SRE cured composites was significantly lower than the counterpart cured by means of traditional processes, with a maximum reduction of 70–80%. After 2010, it was obvious that the researchers have somehow improved the process control of SRE heating process, and the majority of researchers believed that the performance improvement was achieved. But in terms of quantity, except for individual studies [32] that had the improvement over 15%, whether increasing or decreasing, the changing ratios of others were basically around 5%. While some of the test results such as by Fukuda [25], Athanasopoulos [28], and Hayes [31], all indicated that although the strength of SRE cured samples decreased compared to oven cured one, the modulus improved, and some of them believed that this result was caused by higher curing degree of SRE heating process. Enoki [29] conducted the single fiber tensile tests with the SRE heated and unheated single carbon fiber, and a slightly increased strength of SRE heated carbon fiber was obtained, which meant the electrical current had no undesirable effect on the tensile load performance of carbon fiber. Only 6 studies gave the clear mechanism explanation for the test results. But part of the explanation was about improper process parameters or lax variable control such as curing pressure, heating rate, and auxiliary materials. In general, it can be concluded that existing researches suggested that the ultimate mechanical performance of SRE cured CFRP parts was determined by the curing temperature field and forming pressure during the SRE curing process, which was from the point of view of the resin matrix quality. However, the influence of fiber self-heating mechanism on the specific performance like interfacial strength might not be clearly revealed. Therefore, mechanical performance of SRE cured CFRP parts is still indefinable if the mechanism explanation was only according to a single type of mechanical test result, or only considered a single process factor.

Table 1 Reviewed mechanical performance results of different types of SRE heated samples compared to traditional method processed samples in literatures

Time	Researcher	Material	Test	Strength (MPa)			Modulus (GPa)			Mechanism explanation
				SRE	Oven	Imp.	SRE	Oven	Imp.	
1990	Moriya [24]	Unidirectional carbon/epoxy prepreg	Tension	1730	–	–	–	–	–	–
1994	Fukuda [25]	CF/epoxy prepreg sheeting	Flexure	968	1071	− 9.6%	81.4	67.5	+ 20.6%	Inserting copper reduced interlayer strength
1999	Joseph [26]	CF/pitch and CF/PAN	Flexure	520	773	− 32.7%	12.7	35.1	− 63.8%	–
2005	Naskar [27]	CF/polyetherimide	Tension	670	2277	− 70.6%	22	140	− 84.3%	Lack of pressure led to voids and defects
2010	Athanasopoulos [28]	UD Sigrafil/E022 Prepreg UD T700S -SCRIMP	Tension	1580.0 1826.2	1601.4 1810.0	− 1.3% + 0.9%	125.1 107.1	122.5 108.8	− 2.1% − 1.6%	–
2012	Enoki [29]	Single CF	Tension	3.30	3.18 (unheated)	+ 3.7%	–	–	–	–
2014	Zhang [30]	Unidirectional carbon fiber fabric/epoxy	Flexure ILS	807.7 45.3	– –	– –	105.2 –	– –	– –	Fast heating rate reduced performance
2015	Hayes [31]	CF/epoxy prepreg	Flexure	810	850 (oven) 890 (autoclave)	− 4.9% − 9.0%	49.5	43 (oven) 49 (autoclave)	+ 15.1% + 10.2%	Higher curing degree led to higher modulus
2015	Ashrafi [32]	Carbon/epoxy prepreg	Lap shear (kN)	12.5	7.5 (oven) 12.1 (autoclave)	+ 66.7% + 3.3%	–	–	–	–
2016	Ashrafi [33]	Carbon/epoxy scarf	Tension	192.2	183.9	+ 4.5%	–	–	–	Uniform temperature prevented the surface overheating
2017	Xu [34]	GF/CNT film (37% epoxy)	Tension	550	545	+ 0.4%	23.5	22.6	+ 3.9%	–
2017	Smith [35]	Graphite/epoxy prepreg	Lap shear (kN)	7.9	–	–	–	–	–	–
2018	Liu [36]	GF/PP prepreg + CF veil	Flexure	425	442	− 3.85%	21.8	22.6	− 3.75%	Low pressure and high viscosity caused high porosity in carbon veil

In this work, the major aim is to reveal the effect mechanism of SRE heating process on the mechanical properties of the CFRP laminated parts. A series of curing experiments and process investigations for different heating rate were conducted. Comprehensive mechanical tests such as tension, compression, flexural, and interlaminar shear (ILS) were carried out. Then, by means of morphological characterization, the void content and resin flowing behavior were discussed, and the interfacial morphology was further characterized. From the different test results, the relationship among the different types of mechanical properties was analyzed. Finally, the mechanism explanation considering multiple process factors influencing the mechanical performance was given.

2 Experiments

2.1 Material and equipment

The composite system UIN10000/T800 unidirectional prepreg (China Weihai Guangwei composite co., LTD) with a resin content of 30% and a thickness of about 0.1 mm per layer was employed in this study, which is a typical carbon fiber reinforced material system used in aerospace industry. The recommended cure cycle for this system (part thickness < 5 mm) is based on a preliminary ramp at 1–2 °C/min from room temperature to 120 °C, followed by an isothermal stage at 120 °C for 90 min. The final cycle is based on a cooling stage from 120 °C to room temperature (natural cooling). The curing process was performed under vacuum bag pressure of 0.095 MPa. The 10 mm wide red copper strip (Hengxu hardware co., LTD) with the purity of 99.7% was adopted as the electrode. The soft copper cables with a cross area of 60 mm^2 (maximum current 300 A) were used as the heating transmission lines, which had connectors in both ends for a quick plugging operation. An aluminum alloy plate with a side length of 500 mm was used as the curing mold. In the SRE curing process, the polyimide film (Meixin insulation materials Co., LTD) was used for insulating between the composites and the metal mold. Other supporting materials used in the experiment were purchased from supplier Airtech co., LTD, such as L500Y vacuum bag, PMMA release film, B150 breather, and RP3 perforated released film.

The self-developed automatic temperature control power supply based on a commercial DC high-power supply (SZPAIER co., LTD) was employed for SRE curing process. The maximum output electricity of the power supply was 300 A, and the rated power was 4.50 kW. The power supply can be controlled according to the temperature input signal both in constant current and voltage modes. For fabricating the comparative experimental samples, the curing oven (Shanghai Boxun Co., LTD) with the inner dimension of 600 × 600 × 800 mm was used.

2.2 Temperature distribution field characterization

Before the formal curing experiment, the SRE heating temperature field under different process parameters was observed by the infrared thermal image camera (Flir A300). Five different electrode arrangements and the corresponding temperature distribution images are shown in Fig. 1a–e. Different stacking sequences with the same number and the corresponding temperature distribution images are shown in Fig. 1f–j. All images were captured in 30 s after the power supply turned on at a constant power of 80 W.

2.3 Curing arrangement and methodologies

The unidirectional laminated composite samples were manufactured for the mechanical tests and their dimensions are shown in Table 1. There are four types of testing sample respectively corresponding to tension, compression, flexural, and ILS test, and samples of each types were cured in five batches by five curing experiments that had the different heating parameters: oven 1 K/min (recommended process), SRE 1 K/min, 3 K/min, 5 K/min, and 10 K/min (Table 2). In all experiments, the same vacuum bagging (at − 0.095 MPa) arrangement was applied as shown in Fig. 2. A layer of polyimide film was matted between the aluminum alloy mold for insulation. Besides, red copper strips were welded and then embedded into the edge of every two layers of CFRP parts. In SRE curing process, two cables were connected with electrodes and sealed by the sealing tape. The infrared thermal image camera was used to observe the temperature distribution. The curing energy consumption of all curing experiments (including the oven process) was measured by a power meter connected to the main power circuit.

2.4 Physical and mechanical characterization

2.4.1 Void content

The void content of samples was characterized by optical microscopy (BMM-50E, BIMU, China). The measurement results of each sample were obtained according to 18 non-overlapping images captured from three different sections. In addition, to reveal the resin flow behavior, the microscopy was also used to observe the surface morphology of the samples cured by different curing methodologies.

2.4.2 Mechanical performance tests

The tension, compression, flexural, and ILS tests were conducted respectively based on the standard of ASTM D3039/D3039M [37], D6641/D6641M [38], ASTM D7264/

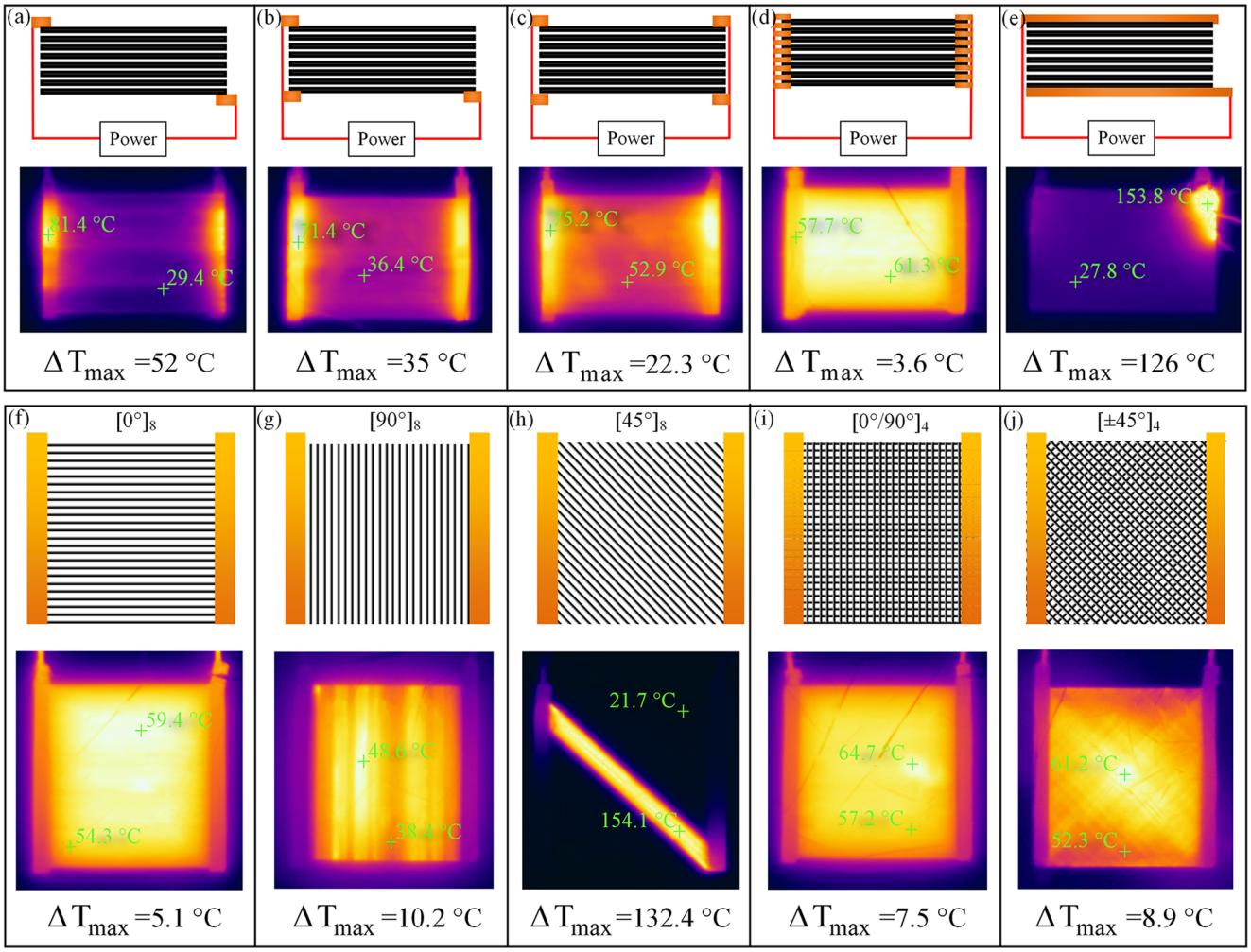

Fig. 1 Different electrode arrangement (**a**–**e**) and their corresponding temperature distribution infrared images; different prepreg stacking sequence (**f**–**j**) and their corresponding temperature distribution infrared images

D7264M [39], and D2344/D2344M [40]. As shown in Fig. 3, all the testing samples were cut from the corresponding unidirectional laminates in sequence, and at least 8 samples of each laminate were tested to ensure testing reliability. The dimension of testing samples was 200 × 20 × 1.6 mm for tension, 140 × 13 × 1.8 mm for compression, 120 × 14 × 2.2 mm for flexure, and 20 × 6 × 2.2 mm for ILS test, and their crosshead speed was 2 mm/min, 1.3 mm/min, 1 mm/min, and 1 mm/min, respectively. Narrow aluminum sheets were bonded using room temperature cure adhesive on the samples of tension and compression, which had a chamfer on the gauge section to reduce stress concentration. An electronic universal testing machine MTS 793 with a 100-kN load cell was used for tensile tests, in which the extensometer was applied. The rest of tests were all conducted on another machine WDW e200d with a 50-kN load cell.

2.4.3 Morphological studies

The cross-section and fracture morphology of SRE heating process cured composites were measured by the Carl Zeiss EVO18 Scanning Electron Microscope (SEM) with a thermionic gun and accelerating voltage of 10 kV. The electron microscope samples with the dimension of 4 × 4 × 2 mm were fixed to the substrate and coated with a 40 nm thickness gold layer to improve the resolution ratio.

Table 2 Geometrical size (mm) of different type and testing samples

Heating rate (°C/min)	Tension	Compression	Flexure	ILS
SRE-1 K/3 K/5 K/10 K, oven 1 K	300 × 300 × 1.6	250 × 250 × 1.8	200 × 200 × 2.2	

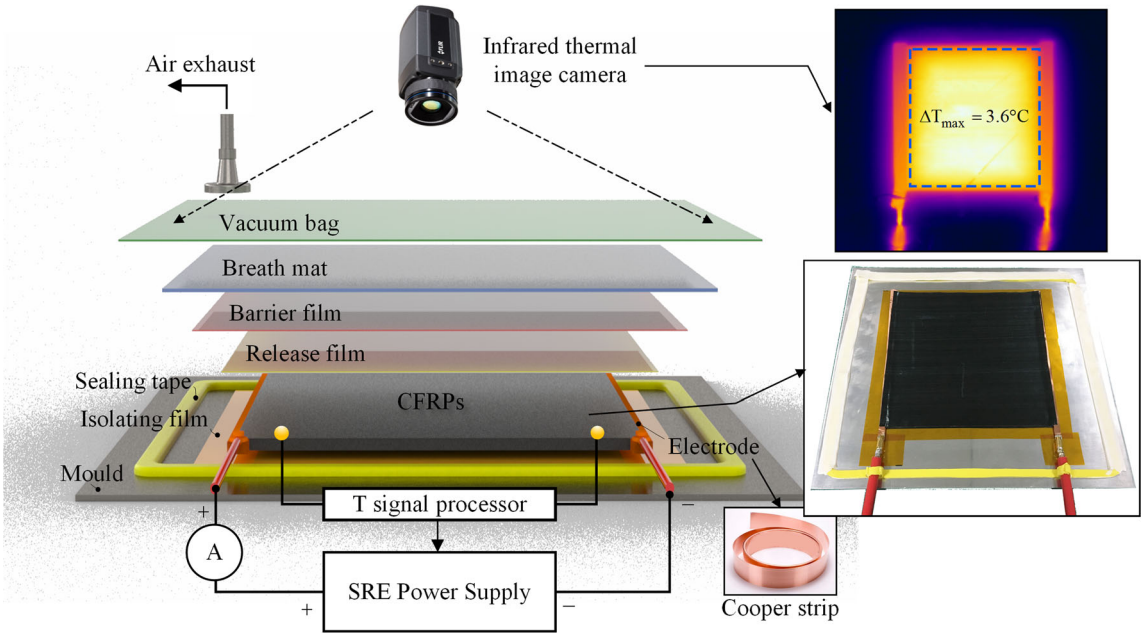

Fig. 2 Vacuum bagging arrangement used in SRE heating/curing process

3 Results and discussion

3.1 Temperature distribution field and curing efficiency assessment

As shown in Fig. 1a–e, the temperature uniformity in-plane becomes more uniform as the increase of the number of interlayer electrodes. This is because that the contact resistance between the copper and the prepreg is much smaller than that between two carbon fiber prepreg layers. In order to reduce the heat at the electrode contact area, the current passing through the thickness direction of laminates must be minimized as much as possible. Therefore, the arrangement of 1-copper/2-prepreg was adopted for curing experiments. As shown in Fig. 1f–j, the result that has the most uniform temperature field was obtained from the 0° stacked one, and the 45° stacked laminates could barely be heated uniformly. The 0°/90° laminate also achieved a preferable results during the whole curing process. For results of 90° and ± 45° laminate, although the striped or intersected hot areas can be observed initially, as the temperature goes up, their temperature fields were eventually improved just as good as that of 0° laminate.

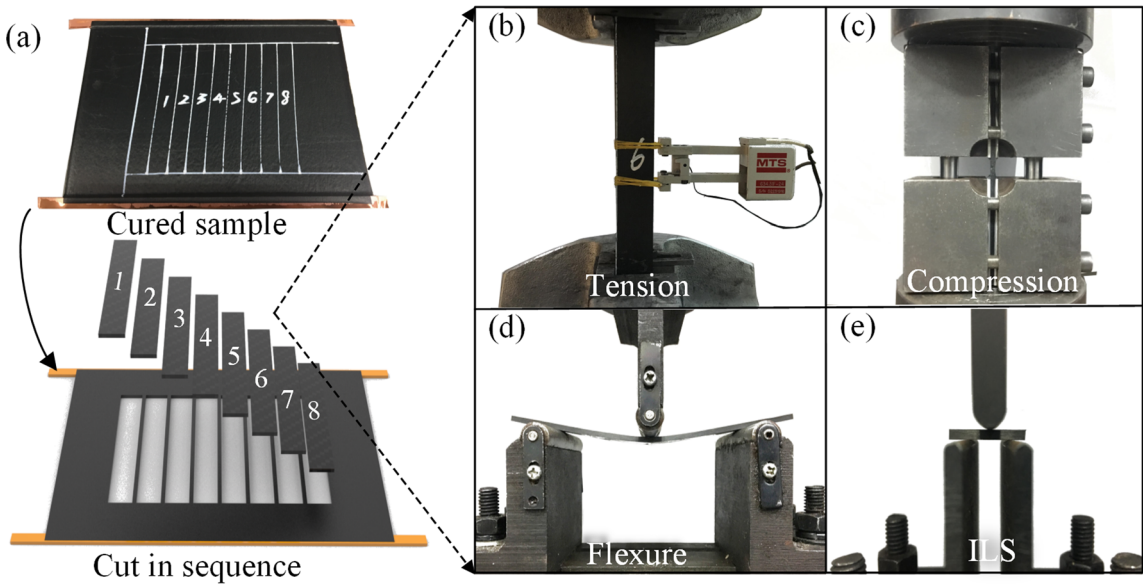

Fig. 3 **a** The schematic diagram of sample cutting and experimental photos of **b** tension, **c** compression, **d** flexure, and **e** ILS tests

This indicates that every fiber in the laminates being conducted can generate a uniform temperature field, and the flowing hot resin leads to more overlap between the fibers, which can further homogenize the temperature field.

The result of time consumption of different processes is shown in Table 3. For SRE processes, in addition to the shorter heating time, the rapid cooling rate also made contribution to the cycle shortening. This is because all SRE curing experiments were conducted in the open (no cavity) environment instead of an adiabatic cavity. Therefore, even for the same heating rate of 1 K/min, the total curing time of SRE process can be reduced 32.8% of that of oven process. The fastest curing process namely the SRE10K/min process achieved 61.5% time saving compared to oven process. The typical temperature curves of SRE 10 K/min and oven 1 K/min are shown in Fig. 4a. The SRE process realized the temperature tracking error within 1 °C, but the oven always kept a temperature lag of 5 to 10 °C. This can be attributed to the fact that the CFRP part was volumetrically heated and the temperature had the rapid response to electrical current conducting in the fiber.

As shown in Fig. 4b, the consumption of oven processes for the parts with different size basically had the same energy consumption level of 3.0 kW h, which is due to the limited effect of the part size in this work on the heat flowing inside the oven. Nevertheless, the size of parts obviously affected the SRE process, and the tension sample with the largest heat dissipation area reached the maximum energy consumption. Considering the energy efficiency, as compared in Fig 5 a and b, a large amount of useless energy was used to heat air, mold, cavity wall, and auxiliary materials in oven process. On the contrary, for SRE heating process, under the heat insulation measures, the electrical energy was completely converted into thermal energy, and very little heat dissipated into the environment. As a conclusion, the reason of low energy consumption, short cycle for SRE heating/curing process can be attributed to the rapid temperature response, fast cooling rate, and high energy usage efficiency.

3.2 Void content and surface analysis

The void content and thickness of different samples and the corresponding cross-section images are illustrated in Fig. 6. The void content of SRE 1 K sample achieved the reduction of

Table 3 Actual curing time (min) of different curing processes

Time (min)	Oven 1 K	SRE 1 K	SRE 3 K	SRE 5 K	SRE 10 K
Heating	100	100	34	20	10
Dwell	90	90	90	90	90
Cooling	127	23	24	24	22
Total	317	213	148	134	122
Time saved	–	32.8%	53.3%	57.7%	61.5%

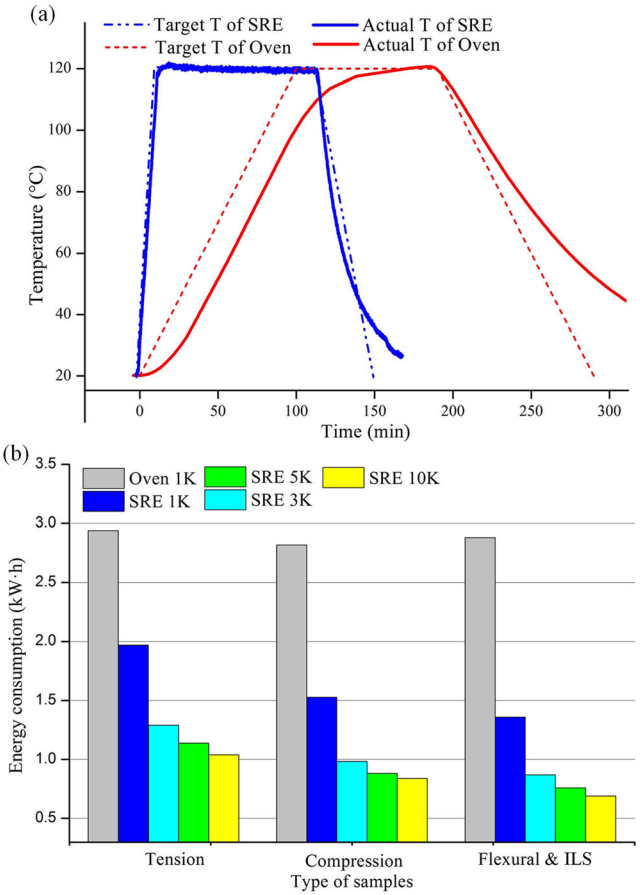

Fig 4. **a** Typical temperature curves of the SRE 10 K/min and oven 1 K/min process. **b** Energy consumption bar graph of different curing processes

17.25% compared with the oven 1 K sample. This is because the uniform temperature distribution enabled the uniform flow of the resin, and the void was supposed to be more easily removed. But with the increase of the heating rate of the SRE process, the void content was gradually raised. This can be explained as the shorter heating time led to the decrease of the resin flow time, and the resin did not effectively wet-out the fibers bed and the void was not able to be eliminated in time [41]. Generally, void content determines the quality of the resin matrix, which may further affect the interlayer bonding strength. The results of material thickness are similar to the distribution of void content, which further indicates that the resin flow time is affected by the heating rate. The difference in thickness also leads to the difference in fiber volume content, but the difference in fiber content in all samples was only around 1%.

The surface morphology of the different CFRP samples can reveal the resin flow behavior under different heating rate more intuitively. As shown in Fig. 7a, for the uncured CFRP prepreg, the clumped resin was unevenly distributed on the surface of dry fiber. In the process with the recommended heating rate of 1 K/min, as shown in the Fig. 7 b and c, the

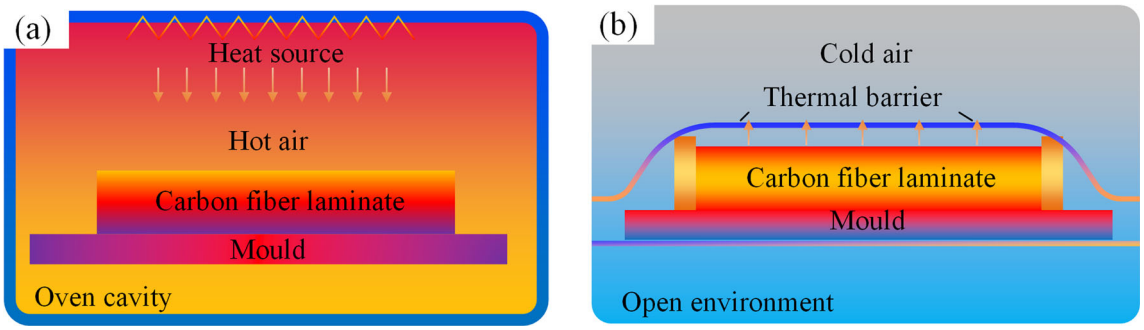

Fig 5. Schematic diagrams of heat transfer mechanism corresponding to **a** oven heating process and **b** SRE heating process

resin was evenly coated on the fiber surface with only a small number of void spots. This means that under the pressure of the vacuum bag, the resin expectably flowed along the pressure passage and filled gaps between fiber. However, although the resin viscosity reached the same low magnitude during the other SRE process with higher heating rate, the shorter resin flowing time was not enough for the full impregnating. As shown in Fig. 7f, the SRE 10 K sample had the inferior surface quality, and due to the high void content between the layers, it was about 1.3% thicker than the other samples. Predictably, if there is no other unknown factor, the final mechanical properties will be directly related to the void content results. However, the results of mechanical tests did not follow this preconceived rule.

3.3 Mechanical performance

Before the mechanical tests, the degree of cure was characterized by the DSC (Differential Scanning Calorimeter), and all the samples nearly achieved 100% polymerization (because

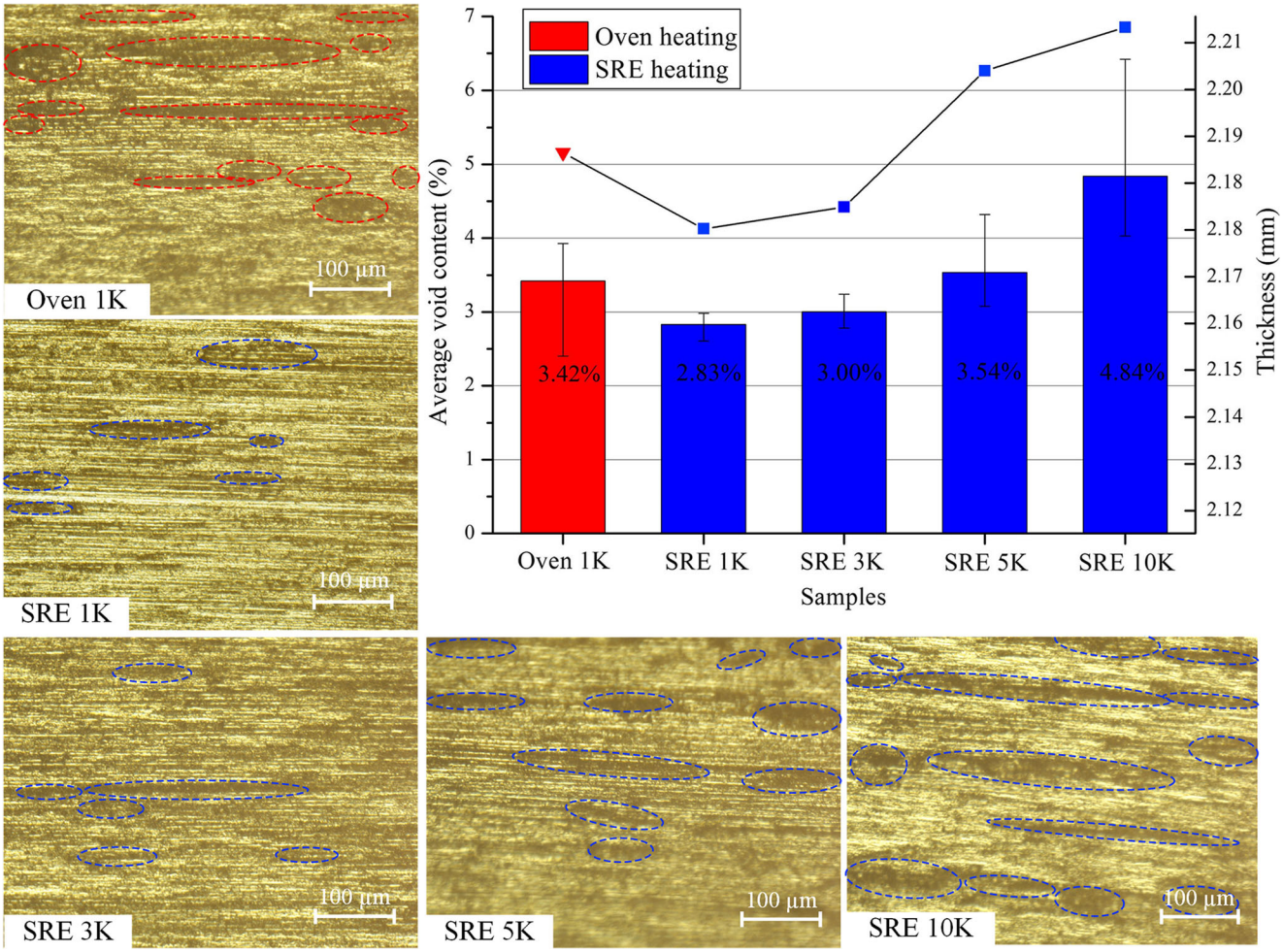

Fig. 6 Chart of sample s thickness and void content and the corresponding cross-sectional micrographs

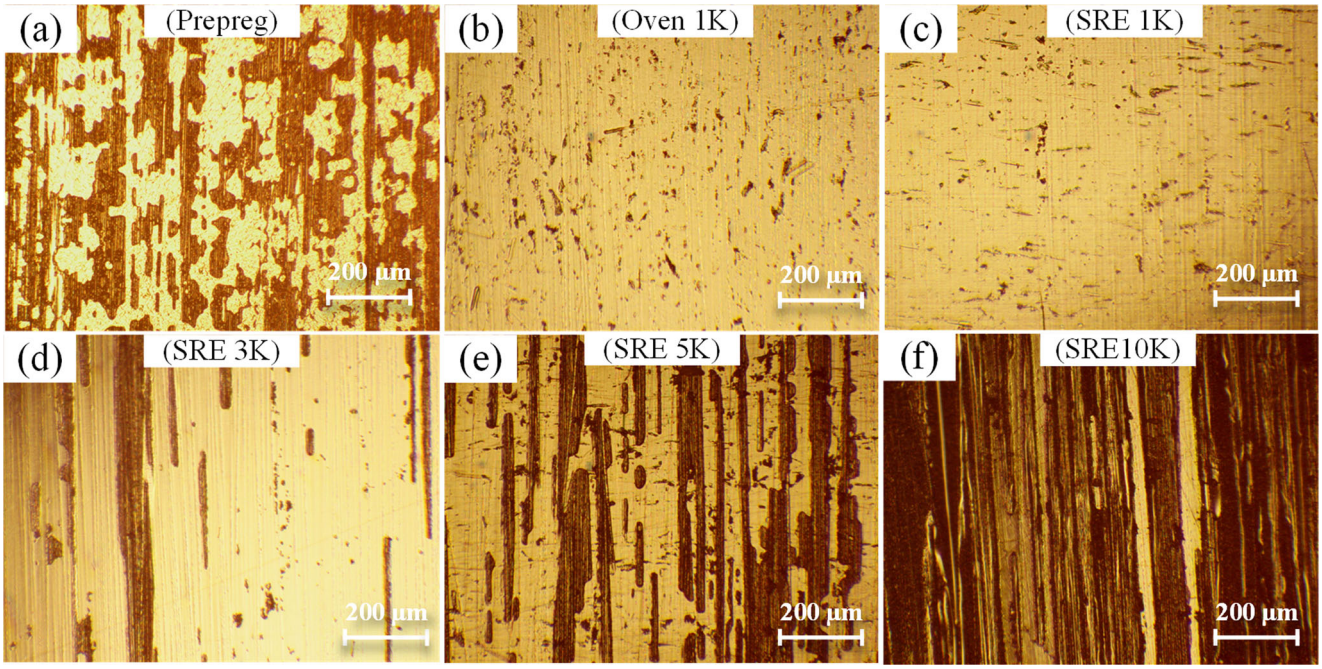

Fig. 7 **a**–**f** Micrographs of resin-fiber distribution on surface of different samples

all the experiments adopted the same dwelling of 90 min). In order to comprehensively characterize the longitudinal, in-plane, matrix, and the interlayer strength of samples cured by oven and SRE heating processes, the most typical tests including tension, compression, three points bending, and ILS were respectively conducted.

3.3.1 Tensile strength

The tension test results of the samples are shown in Fig. 8. It can be clearly verified in the tensile strength column chart that the tensile strength of samples cured by the SRE processes was all higher than that of oven cured sample, and SRE 3 K sample with the highest strength achieved an improvement of 69.23% compared to sample of oven 1 K. In terms of tensile modulus, as shown in Fig. 8b, there was a trend similar to the tensile strength, except for the results of the SRE 10 K sample. The stress-displacement curve of the tensile test shows that the stress continued to increase until the first drop, and then waved up to the maximum. The curve of weaker sample entered the wave stage earlier, and its wave amplitude was greater. It is obvious in Fig. 8d that the fracture surface of the SRE 1 K sample was completely broken with a needle fracture surface, while the oven sample mainly presented the interfacial debonding. This can be concluded that the samples cured by the SRE process may have stronger fiber-matrix interfacial bonding and longitudinal bearing strength than those cured by oven process.

3.3.2 Compression strength

The results regarding to the compression tests are illustrated in Fig. 9, which are vastly different from the tensile test results. As shown in Fig. 9a, the compression strength of the sample cured by SRE 1 K process showed a slight increase compared with that of oven cured sample. However, samples cured by SRE 3 to 10 K processes presented an apparent decrease. Especially, the compression strength of the SRE 10 K cured sample was reduced by nearly half of that of the oven 1 K sample. As shown in Fig. 9, the compression load capacity of the matrix and fibers crashed irreversibly, which corresponded to the sharply dropped stress-displacement curves. Failure photos as shown in Fig. 9a can give an explanation to the result of performance decline. The samples cured by SRE 10 K process were mainly damaged following the delamination between layers, which is totally different from the buckling failure mode of the SRE 1 K sample. This may indicate that the strength of interlayer bonding strength or matrix strength of the sample cured by higher heating rate is weaker, and this result basically agrees with that of void content measurement. However, combined with tensile and bending results, it still cannot explain the mechanism of the effect of the SRE process on mechanical properties compared with the traditional one.

3.3.3 Flexural strength

As shown in Fig. 10, the flexural test results of the samples are illustrated. It is evident in Fig. 10a that the flexural strength of

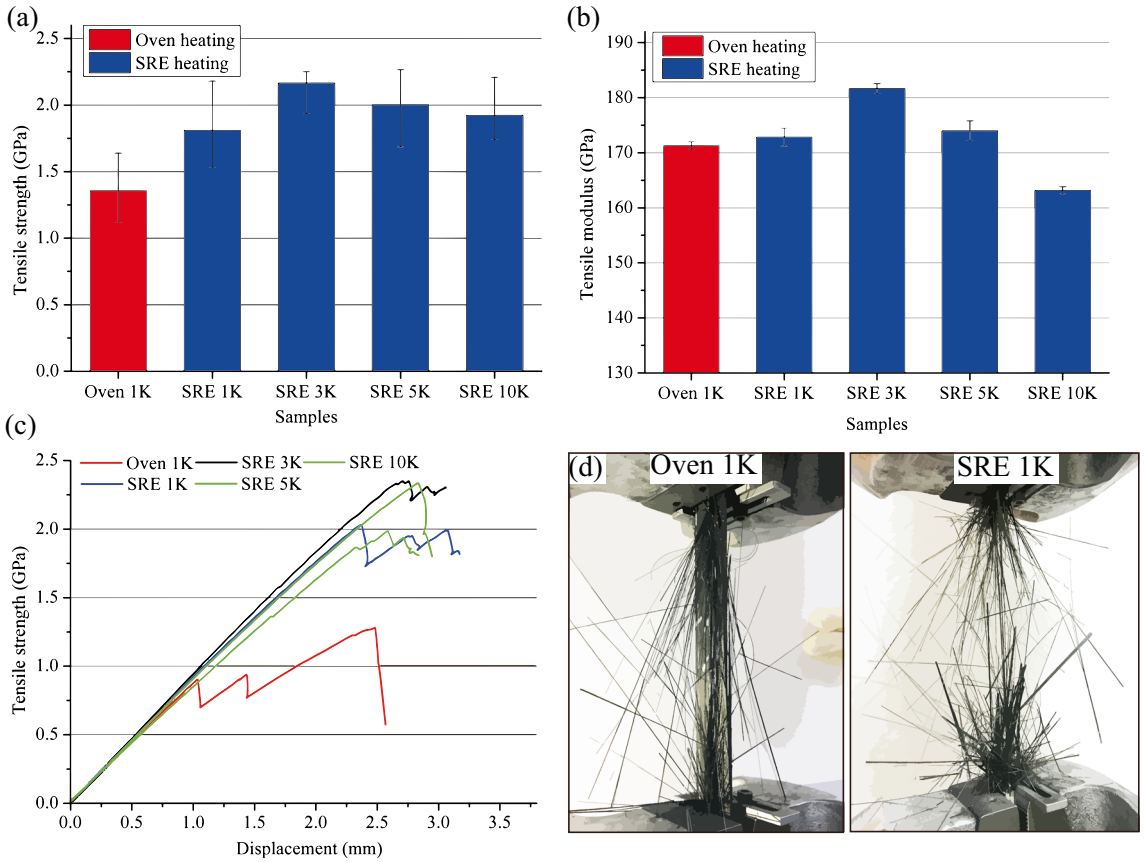

Fig. 8 **a** Tensile strength, **b** modulus column chart, **c** typical tension stress-displacement curves of samples cured by different processes, and **d** the fracture surface appearance of the oven 1 K sample and the SRE 1 K sample

samples cured by SRE heating processes showed a declining trend with the increase of the heating rate. Nonetheless, almost all of the samples cured by SRE heating process performed better in the flexural modulus than that cured by oven heating process, as shown in the Fig. 10b. This result is in agreement with the results of most studies discussed in the introduction. All the stress-displacement curve of flexural tests appeared in the similar variation trend. These curves rose up to the peak at the same slope, and then fluctuated down. When the load rose to the peak, the deformation appeared macroscopic cracks, and after that, as the progressive failure, the fibers broke gradually. This is confirmed in the flexural test failure photos of the samples cured by SRE 1 K and SRE 10 K process as shown in Fig. 10d. For high-performance samples, the fracture appeared from the upper surface namely the compression side, which indicates that the SRE 1 K samples broke in the mode of in-plane shear failure. While the fracture of the SRE 10 K sample was in the mode of in-plane shear crack and central

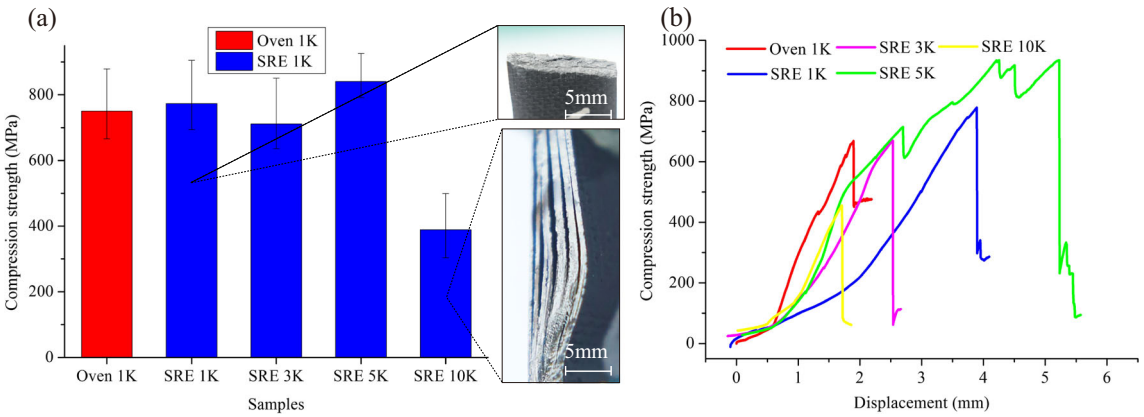

Fig. 9 **a** Compression strength column chart and failure images of SRE 1 K and 10 K and **b** typical compression stress-displacement curves of samples cured by different processes

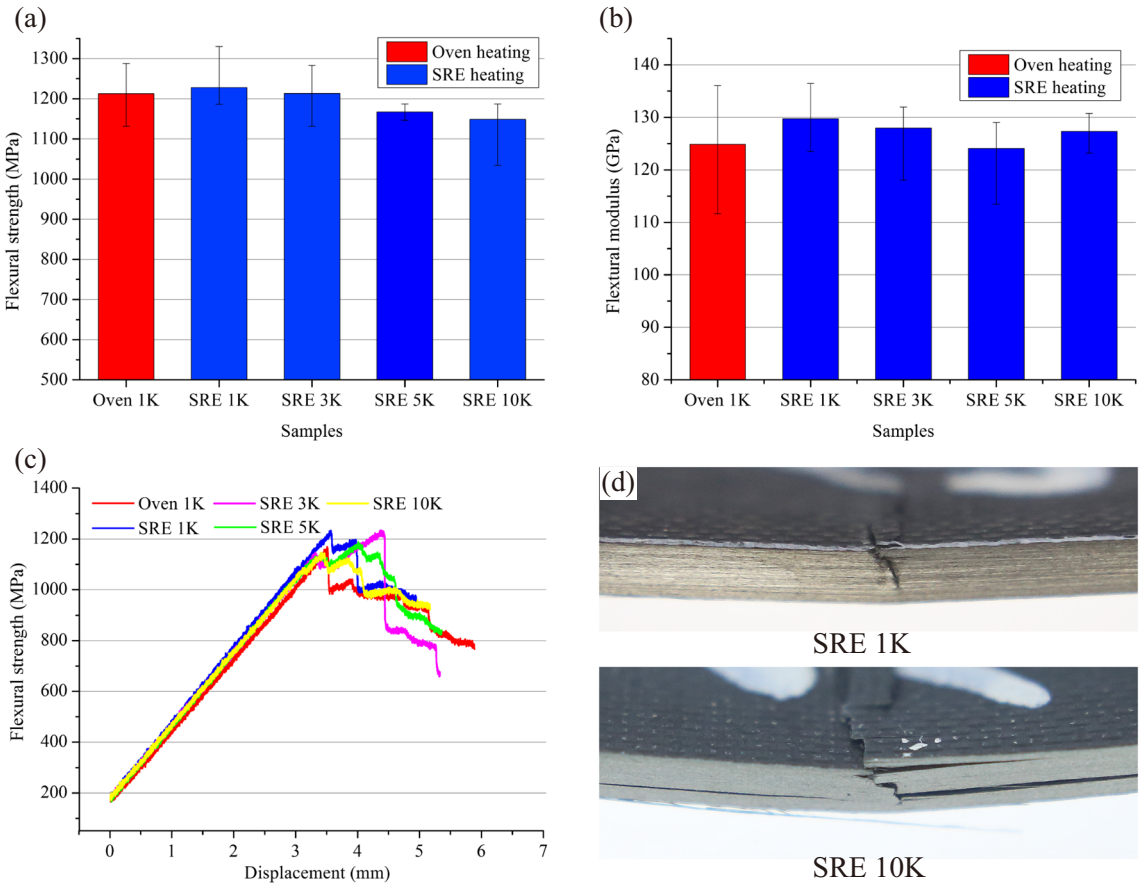

Fig. 10 **a** Flexural strength, **b** modulus column chart and **c** typical flexural stress-displacement curves of samples cured by different processes, and **d** fracture images of SRE 1 K and 10 K.

delamination. Basically, the results of the flexural test also conform to the results of the void content, that is, the higher void content conduced to the weak interlayer matrix property.

3.3.4 Interlaminar shear strength

The ILS tests yielded quite unique results, as illustrated in Fig. 11. It is apparent in the column chart that the ILS strength of all the samples cured by SRE heating processes was higher than that of oven cured sample, and the highest strength was achieved by the sample of SRE 10 K. It can be demonstrated that the upward trend of ILS strength was accompanied by an increase of the heating rate, and this is totally different from results of previous three tests. As dotted squared line in failure photos of Fig. 11b, the SRE 10 K sample broke with few tiny delamination cracks at the middle layer rather than that at the

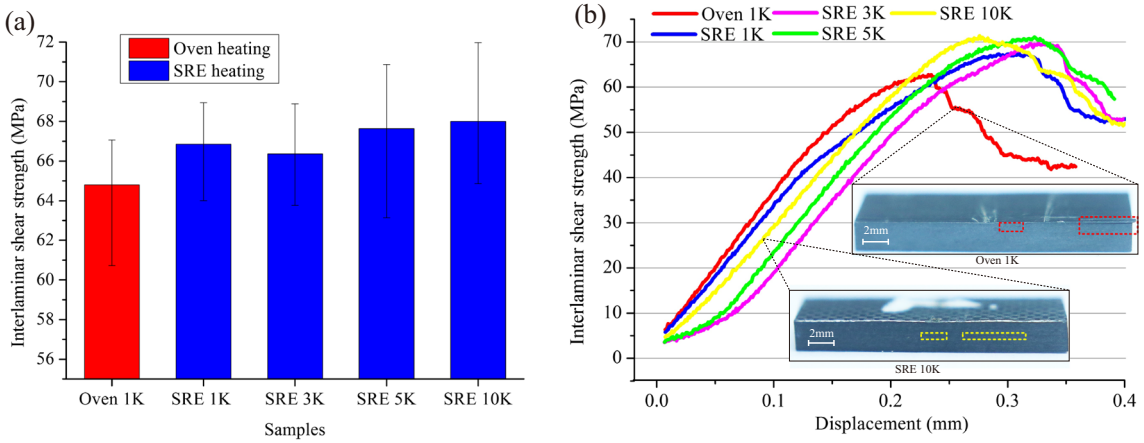

Fig. 11 **a** ILS strength column chart and **b** typical stress-displacement curves of samples cured by different processes and fracture images of SRE 1 K and 10 K

Table 4 Different types of mechanical properties of SRE heated samples compared with the oven 1 K sample

Process	Tension		Compression	Flexural		ILS strength	Average
	Strength	Modulus		Strength	Modulus		
Oven 1 K	–	–	–	–	–	–	–
SRE 1 K	+ 33.08%	+ 0.90%	+ 3.05%	+ 1.29%	+ 3.89%	+ 3.16%	+ 10.15%
SRE 3 K	+ 59.56%	+ 6.03%	− 5.18%	+ 0.058%	+ 2.5%	+ 2.41%	+ 14.21%
SRE 5 K	+ 47.06%	+ 1.58%	+ 12.00%	− 3.73%	− 0.61%	+ 4.38%	+ 14.93%
SRE 10 K	+ 41.18%	− 4.75%	− 48.15%	− 5.27%	+ 1.98%	+ 4.94%	− 1.83%

upper layer close to surface appeared in oven cured sample. Not following the aforesaid rule affected by the void content results, samples cured by SRE 1 K process indicated the worse interfacial property, but the SRE 10 K sample which was cured at higher rate with higher void content performed better in the ILS test. This results may be related to the electrical conductivity of carbon fiber itself as the heat source.

The performance improvement data are listed in Table 4. All the performance of the SRE 1 K cured samples are superior than that of the oven 1 K cured samples but only with 68.7% of total curing cycle and 55% of energy consumption. Although the flexural strength decreases slightly, sample cured by SRE 5 K process achieved the greatest average improvement of 14.93%. However, compression and flexural strength of the SRE sample cured in high heating rate such as 5 K/min and 10 K/min were lower than those of oven cured one, which can be attributed to the high void content and weak interlayer matrix strength. Moreover, all the tension and ILS strength of SRE cured samples were higher than those of oven cured samples, which is probably due to the improvement of the fiber-matrix interfacial strength. To verify the conjecture, the micro-morphology of fiber-matrix interfacial area is discussed down below.

3.4 Cross-section and fracture morphology characterization

The SEM micrographs of cross-section (cut along the fiber axis) and snapped fracture of the different samples are shown in Fig.12a–e and Fig.12f–j, respectively. The yellow dotted line squared area in Fig. 12b–e demonstrates the shape of the resin coated on the fiber. Some of them are tightly attached to the surface of the fiber, some filling the fiber grooves or gaps between the fibers. However, in the micrograph of oven cured sample, there was no distinct resin being found on the fiber surface, and only scattered resin particles were distributed between fibers as enlarged in the Fig. 12a. This suggests that the fiber-resin interfacial strength of oven cured sample was not strong enough to resist the shear force during cutting process. Then focusing on the fracture morphology, for oven 1 K cured sample, there were a large number of bare fibers and neat resin holes on the whole surface, which illustrated that the fiber-resin interfacial strength was weak. On the contrary, a large amount of resin adhered on fiber surface can be found in SRE cured samples as red dotted line circled in Fig. 12g–j. Especially in the samples of SRE 3 K, the muciform resin fully fill the fiber gap and was not separated from the fiber,

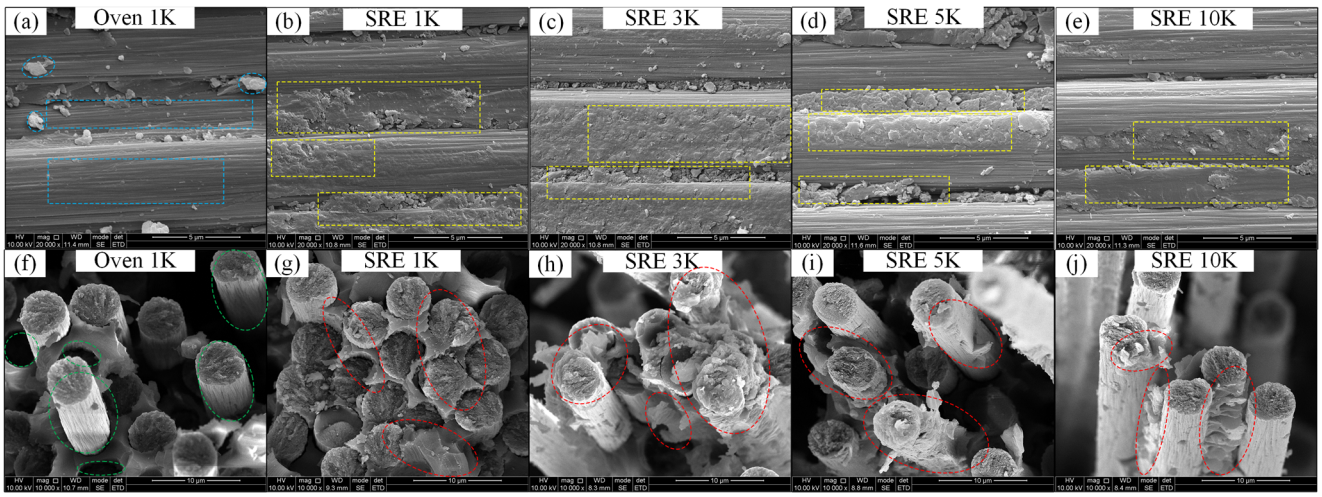

Fig. 12 Cross-section SEM micrographs of **a** oven 1 K, **b** SRE 1 K, **c** SRE 3 K, **d** SRE 5 K, and **e** SRE 10 K; Fracture SEMs of **f** oven 1 K, **g** SRE 1 K, **h** SRE 3 K, **i** SRE 5 K, and **j** SRE 10 K

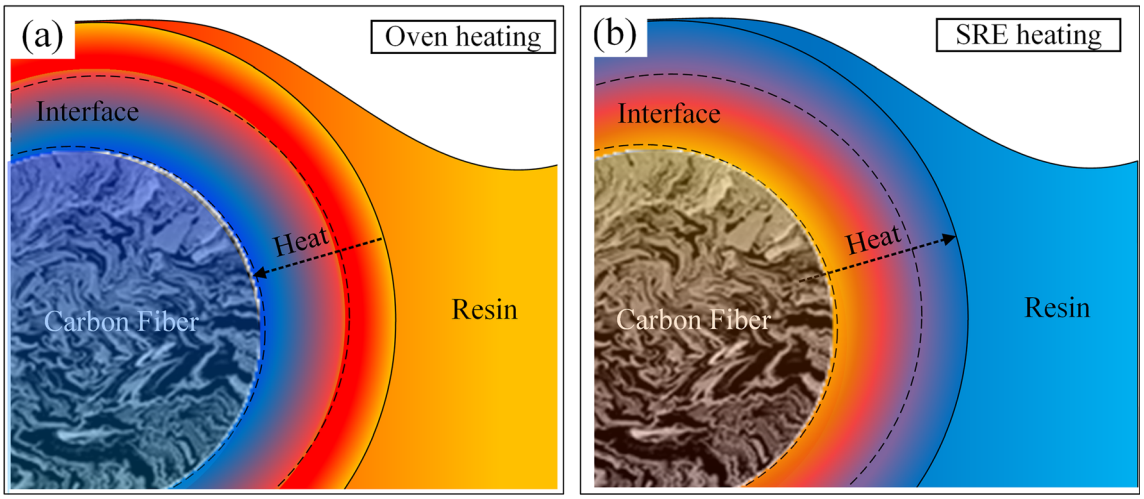

Fig. 13 Fiber-resin interface heat transfer mode diagrams of **a** external heat source in oven heating and **b** fiber heat source in SRE heating

and the cataphracted resin on fiber can also be found in the sample of SRE 10 K. Basically, the conclusion can be made from the above results that for the SRE processes with higher heating rate, the increase of tensile and ILS strength is due to the enhancement of fiber-matrix interfacial strength, while the decrease of compression and flexural strength is due to the higher void contents and the consequent weaker matrix strength.

The mechanism of interface strength enhancement can be explained as follows. The heat transfer modes along the fiber-resin interface are shown in Fig. 13. In both heat transfer modes, temperature gradients of different directions are formed along the interface. But in SRE heating process, when the fibers as the heat source, as shown in Fig. 13b, there must be a temperature difference. The heating rate on the fiber-resin interface is much higher than that of the macroscopical parts, so the temperature difference along interface is relatively larger. This large temperature difference can lead resin around the interfacial area to be heated and cured preferentially, and this prior curing can significantly increase the curing quality and bonding strength of resin around the interfacial area. The similar mechanism of interfacial strength enhancement was also reported in microwave [42] and SRE heating process [43].

4 Conclusion

The literature review summarized most of existing studies on mechanical performance of SRE heating cured CFRP parts in chronological order. Comparing with the traditional curing method, some of the existing mechanical performance results of SRE cured samples were enhanced, but some were weakened. The mechanism explanations were mainly based on a single type of mechanical test or result.

In this work, a series of oven and SRE curing experiments with different heating rate were conducted. Comprehensive mechanical tests including tension, compression, flexure, and ILS tests were carried out. By means of morphological characterization, the void content and resin flowing behavior were analyzed, and the interfacial morphology was characterized. SRE curing process with the heating rate of 1 K/min thoroughly increase all the sample's mechanical performance compared to oven process. For SRE processes with higher heating rate, the tensile and ILS strength were increased because of the enhancement of fiber-matrix interfacial strength, but the compression and flexural strength were decreased because of the higher void contents and the consequent weaker matrix strength. Several concise conclusions are summarized below:

1. Curing time and energy consumption of SRE heating process can be significantly reduced compared to that of the oven process due to the extremely fast heating/cooling rate and the efficient utilization of electrical energy.
2. SRE heating process resulted in lower void content due to the uniform temperature field, but the insufficient resin flowing in the process of rapid heating rate leaded to high void content and weaker matrix strength.
3. Fiber-resin interfacial strength was markedly improved for SRE heating process because the fiber preferential heating effect in fiber-matrix interfacial area.
4. This work presented the mechanisms both for the improvements and reductions of some certain mechanical properties, which may be possible to explain the results in some existing literature and to provide guidance for further development of the SRE process. In order to improve the matrix strength, the optimization of implementing the resin flowing dwelling during rapid heating process can be further considered.

Acknowledgments The authors sincerely appreciate the continuous support provided by our industrial collaborators.

Funding information This work was supported by the National Natural Science Foundation of China (Grant no. 51775261) and Postgraduate Research and Practice Innovation Program of Jiangsu Province (KYCX18_0319).

References

1. Bortoluzzi DB, Gomes GF, Hirayama D, Ancelotti AC (2019) Development of a 3D reinforcement by tufting in carbon fiber/epoxy composites [J]. Int J Adv Manuf Technol 100:1593–1605
2. Hassan MH, Othman AR, Kamaruddin S (2017) A review on the manufacturing defects of complex-shaped laminate in aircraft composite structures [J]. Int J Adv Manuf Technol 91:4081–4094
3. Witik RA, Gaille F, Teuscher R, Ringwald H, Michaud V, Månson J-AE (2012) Economic and environmental assessment of alternative production methods for composite aircraft components. J Clean Prod 29–30:91–102. https://doi.org/10.1016/j.jclepro.2012.02.028
4. Centea T, Grunenfelder LK, Nutt SR (2015) A review of out-of-autoclave prepregs – Material properties, process phenomena, and manufacturing considerations. Compos Part A Appl Sci Manuf 70:132–154 https://doi.org/10.1016/j.compositesa.2014.09.029
5. Nele L, Caggiano A, Teti R (2016) Autoclave cycle optimization for high performance composite parts manufacturing. Procedia CIRP 57:241–246. https://doi.org/10.1016/j.procir.2016.11.042
6. Li YG, Cheng LB, Zhou J (2018) Curing multidirectional carbon fiber reinforced polymer composites with indirect microwave heating. Int J Adv Manuf Technol 97:1137–1147. https://doi.org/10.1007/s00170-018-1974-1
7. Anandan S, Dhaliwal GS, Huo Z, Chandrashekhara K, Apetre N, Iyyer N (2018) Curing of thick thermoset composite laminates: multiphysics modeling and experiments. Appl Compos Mater 25(5):1155–1168. https://doi.org/10.1007/s10443-017-9658-9
8. Struzziero G, Skordos AA (2017) Multi-objective optimisation of the cure of thick components. Compos Part A Appl Sci Manuf 93:126–136. https://doi.org/10.1016/j.compositesa.2016.11.014
9. Song YS, Youn JR, Gutowski TG (2009) Life cycle energy analysis of fiber-reinforced composites. Compos Part A Appl Sci Manuf 40:1257–1265. https://doi.org/10.1016/j.compositesa.2009.05.020
10. Li YG, Li NY, Gao J (2018) Tooling design and microwave curing technologies for the manufacturing of fiber-reinforced polymer composites in aerospace applications. Int J Adv Manuf Technol 70:591–606. https://doi.org/10.1007/s00170-013-5268-3
11. Walczyk D, Kuppers J (2012) Thermal press curing of advanced thermoset composite laminate parts. Compos Part A Appl Sci Manuf 43:635–646. https://doi.org/10.1016/j.compositesa.2011.12.008
12. Park SY, Choi WJ, Choi HS (2010) A comparative study on the properties of GLARE laminates cured by autoclave and autoclave consolidation followed by oven postcuring. Int J Adv Manuf Technol 49:605–613. https://doi.org/10.1007/s00170-009-2408-x
13. Zhou J, Li YG, Li NY, Liu ST, Cheng LB, Sui SC, Gao J (2018) A multi-pattern compensation method to ensure even temperature in composite materials during microwave curing process. Compos Part A Appl Sci Manuf 107:10–20. https://doi.org/10.1016/j.compositesa.2017.12.017
14. Xu XH, Wang XQ, Wei R, Du SY (2016) Effect of microwave curing process on the flexural strength and interlaminar shear strength of carbon fiber/bismaleimide composites. Compos Sci Technol 123:10–16. https://doi.org/10.1016/j.compscitech.2015.11.030
15. Bayerl T, Duhovic M, Mitschang P, Bhattacharyya D (2014) The heating of polymer composites by electromagnetic induction – a review. Compos Part A Appl Sci Manuf 57:27–40. https://doi.org/10.1016/j.compositesa.2013.10.024
16. Riccio A, Russo A, Raimondo A, Cirillo P, Caraviello A (2018) A numerical/experimental study on the induction heating of adhesives for composite materials bonding. Mater Today Commun 15:203–213. https://doi.org/10.1016/j.mtcomm.2018.03.008
17. Kwak M, Robinson P, Bismarck A, Wise R (2015) Microwave curing of carbon–epoxy composites: penetration depth and material characterisation. Compos Part A Appl Sci Manuf 75:18–27. https://doi.org/10.1016/j.compositesa.2015.04.007
18. Yarlagadda S, Kim HJ, Gillespie JW, Shevchenko NB, Fink BK (2002) a study on the induction heating of conductive fiber reinforced composites. J Compos Mater 36:401–421. https://doi.org/10.1177/0021998302036004171
19. Feher L, Thumm M (2004) Microwave innovation for industrial composite fabrication—the HEPHAISTOS technology. IEEE Trans Plasma Sci 32:73–79. https://doi.org/10.1109/TPS.2004.823983
20. Athanasopoulos N, Koutsoukis G, Vlachos D, Kostopoulos V (2013) Temperature uniformity analysis and development of open lightweight composite molds using carbon fibers as heating elements. Compos B Eng 50:279–289. https://doi.org/10.1016/j.compositesb.2013.02.038
21. Athanasopoulos N, Sikoutris D, Panidis T, Kostopoulos V (2012) Numerical investigation and experimental verification of the Joule heating effect of polyacrylonitrile-based carbon fiber tows under high vacuum conditions. J Compos Mater 46:2153–2165. https://doi.org/10.1177/0021998311430159
22. Lupi S (2017) Direct resistance heating.Fundamentals of electroheat
23. Müller B, Palardy G,Teixeira De Freitas S, Sinke J (2018) Out-of-autoclave manufacturing of GLARE panels using resistance heating. J Compos Mater 52(12):1661–1675. https://doi.org/10.1177/0021998317727592
24. Moriya K (1990) Study on fabrication methods of composite structures (1st Report). Joule effect curing of CFRP composite structures and its application to bonding and repair. J Jpn Soc Aeronaut S 38:371–378. https://doi.org/10.2322/jjsass1969.38.371
25. Fukuda H (1994) Processing of carbon fiber reinforced plastics by means of Joule heating. Adv Compos Mater 3:153–161. https://doi.org/10.1163/156855194X00015
26. Joseph C, Viney C (2000) Electrical resistance curing of carbon-fibre/epoxy composites. Compos Sci Technol 60:315–319. https://doi.org/10.1016/S0266-3538(99)00112-8
27. Naskar AK, Edie DD (2006) Consolidation of reactive Ultem® powder-coated carbon fiber tow for space structure composites by resistive heating. J Compos Mater 40:1871–1883. https://doi.org/10.1177/0021998306061300
28. Athanasopoulos N, Sotiriadis G, Kostopoulos V., 2010. A study on the effect of Joule heating during the liquid composite molding (LCM) process and on the curing of CFRP composite laminates. In: Proceedings of 10th international conference on flow processes in composite materials (FPCM10), Ascona, 32.
29. Enoki S, Iwamoto K, Harada R, Tanaka K, Katayama T (2012) Heating properties of carbon fibers by using direct resistance heating. WIT Transactions on the Built Environment 124:239–248
30. Zhang KM, Gu YZ, Li M, Wang SK, Zhang ZG (2014) Resistive heating of carbon fiber aided rapid curing of vacuum assisted resin infusion molding. Adv Mater Res 1030(1032):170–173. https://doi.org/10.4028/www.scientific.net/AMR.1030-1032.170
31. Hayes SA, Lafferty AD, Altinkurt G, Wilson PR, Collinson M, Duchene P (2015) Direct electrical cure of carbon fiber composites. Adv Manuf Polym Compos Sci 1:112–119. https://doi.org/10.1179/2055035915Y.0000000001

32. Ashrafi M, Devasia S, Tuttle ME (2015) Resistive embedded heating for homogeneous curing of adhesively bonded joints. Int J Adhes Adhes 57:34–39. https://doi.org/10.1016/j.ijadhadh.2014.10.002
33. Ashrafi M, Smith BP, Devasia S, Tuttle ME (2017) Embedded resistive heating in composite scarf repairs. J Compos Mater 51:2575–2583. https://doi.org/10.1177/0021998316673706
34. Xu XK, Zhang Y, Jiang J, Wang H, Zhao XL, Li QW, Lu WB (2017) In-situ curing of glass fiber reinforced polymer composites via resistive heating of carbon nanotube films. Compos Sci Technol 149:20–27. https://doi.org/10.1016/j.compscitech.2017.06.001
35. Smith BP, Tuttle M, Devasia S (2017) Embedded resistive heating for bonding of rigid composite structures in space. AIAA SPACE and Astronautics Forum and Exposition, American Institute of Aeronautics and Astronautics.
36. Liu C, Li M, Gu YZ, Gong Y, Liang JY, Wang SK, Zhang ZG (2018) Resistance heating forming process based on carbon fiber veil for continuous glass fiber reinforced polypropylene. J Reinf Plast Compos 37(6):366–380. https://doi.org/10.1177/0731684417751058
37. ASTM D3039 / D3039M-17 (2017) Standard test method for tensile properties of polymer matrix composite materials, ASTM International, West Conshohocken, PA https://www.astm.org/Standards/D3039.htm
38. ASTM D6641 / D6641M-16e1 (2016) Standard test method for compressive properties of polymer matrix composite materials using a combined loading compression (CLC) test fixture. ASTM International, West Conshohocken, PA https://www.astm.org/Standards/D6641.htm
39. ASTM D7264 / D7264M-15 (2015) Standard test method for flexural properties of polymer matrix composite materials. ASTM International, West Conshohocken, PA https://www.astm.org/Standards/D7264.htm
40. ASTM D2344 / D2344M-16 (2016) Standard test method for short-beam strength of polymer matrix composite materials and their laminates. ASTM International, West Conshohocken, PA https://www.astm.org/Standards/D2344.htm
41. Koushyar H, Alavi-Soltani S, Minaie B, Violette M (2012) Effects of variation in autoclave pressure, temperature, and vacuum-application time on porosity and mechanical properties of a carbon fiber/epoxy composite. J Compos Mater 46:1985–2004. https://doi.org/10.1177/0021998311429618
42. Zhou J, Li YG, Li NY, Hao XZ (2017) Enhanced interlaminar fracture toughness of carbon fiber/bismaleimide composites via microwave curing. J Compos Mater 51:2585–2595. https://doi.org/10.1177/0021998316673892
43. Sancaktar E, Ma W, Yurgartis SW (1993) Electric resistive heat curing of the fiber-matrix interphase in graphite/epoxy composites. J Mech Des 115:53. https://doi.org/10.1115/1.2919324
44. Kim M, Sung DH, Kong K, Kim N, Kim B-J, Park HW, Park Y-B, Jung M, Lee SH, Kim SG (2016) Characterization of resistive heating and thermoelectric behavior of discontinuous carbon fiber-epoxy composites. Compos B Eng 90:37–44. https://doi.org/10.1016/j.compositesb.2015.11.037